# The evolved B[e] star HD 87643 : observations and a radiation driven disk-wind model for B[e] stars

René D. Oudmaijer[1], Daniel Proga[1], Janet E. Drew[1], Dolf de Winter[2,3]

[1] *Imperial College of Science, Technology and Medicine, Blackett Laboratory, Prince Consort Road, London, SW7 2BZ, U.K.*
[2] *Dpto. Física Téorica C–XI, Facultad de Ciencias, Universidad Autónoma de Madrid, Cantoblanco, E–28049 Madrid, Spain*
[3] *Centro de Astrofísica de Universidade do Porto, Campo Alegre 823, 4150 Porto, Portugal*

**ABSTRACT**

New high resolution spectroscopic and medium resolution spectropolarimetric data, complemented with optical broad and narrow band imaging, of the B[e] star HD 87643 are presented. The spectrum of HD 87643 exhibits the hybrid characteristics well known to be representative of the group of B[e] stars; a fast wind with an expansion velocity in excess of 1000 km s$^{-1}$ is measured in the hydrogen and helium lines, while a slower component is traced by lower excitation lines and forbidden lines. Clues to the geometry of the rapidly expanding circumstellar shell are provided by the startling polarization changes across H$\alpha$. Comparison with published schematic calculations indicates that the polarizing material is located in a slowly rotating, expanding disk structure. A hydrodynamical model is then presented whose results are consistent with the original two-wind concept for B[e] stars and exhibits kinematic properties that may well explain the observed spectral features in HD 87643. The model calculations use as input a B star undergoing mass loss, surrounded by an optically thick disk. The resulting configuration consists of a fast polar wind from the star and a slowly expanding disk wind. The model also predicts that the stellar wind at intermediate latitudes is slower and denser than in the polar region.

**Key words:** stars: circumstellar matter – stars: individual: HD 87643 – stars: emission line, Be – polarization – hydrodynamics

## 1 INTRODUCTION

The B[e] phase is one of the phases a massive star might go through during its evolution. Since the spectra of such objects are dominated by emission lines, and generally do not show any signs of photospheric absorption lines, it was only due to the work of Zickgraf et al. (1985, 1986, 1996 and references in these papers) on peculiar B-type emission line stars in the Magellanic Clouds that the luminosities of some of these objects began to be known, and their location in the HR-diagram could be plotted with some accuracy.

HD 87643 ($\alpha_{2000} = 10^h 04^m 30^s$, $\delta_{2000} = -58^\circ 38' 52''$; $l=283^\circ$, $b=-2.5^\circ$) appears to be a Galactic counter-part of the B[e] stars in the Magellanic Clouds. Over the last decades spectroscopic studies of the object were reported by Hiltner, Stephenson & Sanduleak (1968), Stephenson (1974), Swings (1974) and Carlson & Henize (1979). The picture that has emerged is that the optical spectrum of HD 87643 is dominated by emission lines from Fe II and the Balmer series, and displays low excitation forbidden lines. Except for blueshifted P Cygni absorption components and interstellar lines no optical absorption lines have been detected. Optical and ultraviolet IUE spectra of HD 87643 are presented by de Freitas Pacheco, Gilra & Pottasch (1982) and de Freitas Pacheco et al. (1985). The UV spectrum appears to be dominated by low ionization absorption lines, although features due to Fe III, Si III and Si IV are present.

McGregor, Hyland & Hillier (1988) find that HD 87643 displays a large near-infrared excess ($J - K \sim 2.6$), which they attribute to hot circumstellar dust. Published broad band photometry indicates variations over long timescales: the $V$ band magnitude was reported as 8.51 in 1968 (Hiltner et al. 1968), and as 9.41 in 1995 (Torres et al. 1995). In the intervening years, the $V$ band magnitude has fluctuated, but an overall trend towards fainter magnitudes is present (Miroshnichenko 1998). No colour information has been published however. The emission line spectrum of the star is also variable. Lopes, Daminelli Neto & de Freitas Pacheco

(1992) show the behaviour of the H$\beta$ line. Its equivalent width (EW) changed by a factor of several in the period 1980 – 1990, reaching a maximum value in 1985.

An interesting aspect of the surroundings of HD 87643 is discussed by Surdej et al. (1981) and Surdej & Swings (1983). They obtained spectra of two high density knots in the large reflection nebula around HD 87643 at offsets from the star of 20$''$ NW and 17$''$S. Surdej & Swings (1983) show that the central peak H$\beta$ emission at the two positions differs by about 150 km s$^{-1}$, and argue that the observed velocity difference confirms their hypothesis that the line forming region is not isotropic.

The layout of this paper is as follows; Sec. 2 describes our observations of the star. Sec. 3 describes key features of the optical spectrum, and then Sec. 4 discusses the polarization of the object. Constraints on the distance and hence on the evolutionary status of the object are provided in Sec. 5. Then in Sec. 6 a new dynamical model for the inner circumstellar environment of HD 87643 and B[e] stars in general is outlined. A virtue of this model is that it offers great promise of fitting in with the striking spectropolarimetric behaviour at H$\alpha$ seen in HD 87643. The paper's conclusions appear in Sec. 7.

## 2    OBSERVATIONS

### 2.1    Echelle spectroscopy

Spectroscopic data were obtained during the nights of 20 and 21 April 1997 employing the Coudé echelle spectrograph on the 74$''$ telescope of Mount Stromlo Observatory. The observational set-up included a 2 arcsec slit, the 300 lines/mm cross-disperser grating and a 2K × 2K TEK CCD. Since the cross-disperser is not located in the pupil plane, vignetting occurs away from the central order. Hence, the CCD was windowed during read-out. To improve signal-to-noise, the data were binned over two pixels in both the dispersion and cross-dispersion directions.

On 20 April, observations at a central wavelength of 6562 Å were obtained. The total on-source integration time was 45 minutes, obtained in 3 individual exposures of 15 minutes each. Observations of a bright B star (HR 4199, B0V) were also obtained to correct the spectrum for telluric absorption lines, and Th-Ar arc maps were obtained for the dispersion correction. The dispersion fit through more than 450 identified lines yielded an rms value of 0.009 Å using 4$^{\rm th}$ order polynomials in both the dispersion and cross-dispersion direction. The final spectrum consisted of 20 different orders covering the range from 5750 to 7220 Å, with a spectral resolution as measured from telluric absorption lines of 8.5 km s$^{-1}$. The data were corrected for telluric absorption by matching the strength of the absorption lines with those in HR 4199.

On 21 April, two 15 minute exposures in the blue at a central wavelength 5000 Å were obtained. The spectra contained 33 orders, and covered a wavelength range from 4270 – 5705 Å. Due to shorter exposure times and the reddening of the object, the blue spectrum has a lower signal-to-noise (SNR) than the red spectrum.

Data reduction was performed in IRAF (Tody, 1993), and included the steps of bias subtraction, flatfielding, background subtraction and wavelength calibration.

### 2.2    Spectropolarimetry

Optical linear spectropolarimetric data were obtained using the RGO Spectrograph on the 3.9-metre Anglo-Australian Telescope on 31 December 1996 and 1 January 1997. The weather was clear.

The instrumental set-up included a half-wave plate rotator set to various angles to obtain the Stokes QU parameters and a calcite block to separate the light leaving the retarder into perpendicularly polarized light waves. Two holes in the dekker allow for simultaneous observations of the object and the sky. Four spectra are recorded, the O and E rays of the target object and the sky respectively. One complete polarization observation consists of a series of consecutive exposures at four rotator positions. Spectropolarimetric standards were observed during both nights. The instrumental polarization was found to be negligible.

A 1024 × 1024 pixel TEK-CCD detector was used which, combined with the 1200V grating, yielded a spectral coverage from 6340 – 6880 Å, in steps of 0.54 Å. Wavelength calibration was performed by observing a Cu-Ar lamp before each exposure. On 31 December 5 × 4 sets of data were taken with exposure times of 90 s, a day later 3 × 4 sets with exposure times of 120 s were obtained. A slit width of 1.5 arcsec was used.

The initial processing of the data was performed in the IRAF package. After bias-subtraction and flatfielding, the individual spectra were extracted by tracing the pixel rows containing the data. The wavelength calibration was performed by fitting a 3$^{\rm rd}$ order polynomial through more than 20 identified lines in the arc spectra, and resulted in dispersion fits with a $\sigma$ of 0.07 Å. The resulting spectral resolution as measured from arc lines is 60 km s$^{-1}$. The E and O ray data were then extracted and imported into the Time Series/Polarimetry Package (TSP) incorporated in the FIGARO software package maintained by STARLINK. The Stokes parameters were determined and subsequently extracted.

### 2.3    Imaging

Images of HD 87643 were obtained through $V$, $R$, H$\alpha$ and [S II] filters with the Dutch 92 cm telescope stationed at the ESO La Silla. On 12 July 1992 images were taken through the $R$ (ESO#421), H$\alpha$ (ESO#387) and [S II] (ESO#391) pass-bands for 4 × 3, 3 × 30 and 3 × 70 sec, respectively. The detector used was a GEC 576 × 385-pixel CCD. The pixels have a size of 22 $\mu$m corresponding to 0.36 arcsec on the sky. On 20 April 1995 six images of 10 sec were obtained with the ESO#420 $V$ filter. In this case, the CCD was a Tektronix 512 × 512 pixels CCD, with a pixelsize of 27 $\mu$m corresponding to 0.44 arcsec.

After the images were corrected for bias, cleaned of cosmic ray hits, and flatfield-corrected, the images were aligned and co-added. The seeing measured from Gaussian fits to field-star images corresponded to a full-width-at-half-maximum (FWHM) of 1.8 arcsec.

## 3    THE OPTICAL SPECTRUM

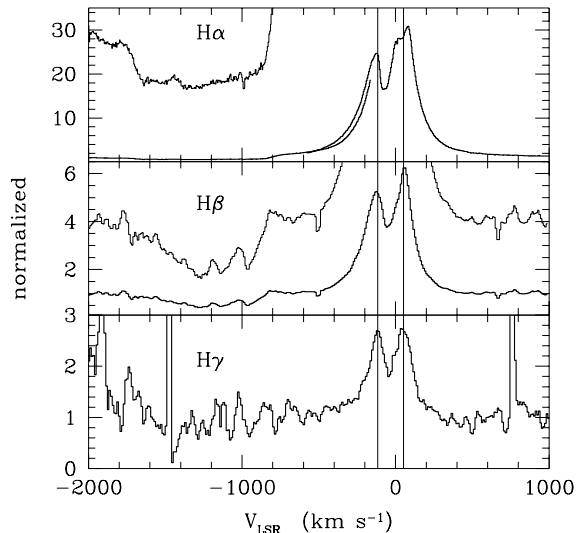The optical spectrum is dominated by permitted and forbidden emission lines of Fe II, and the Balmer lines. Some
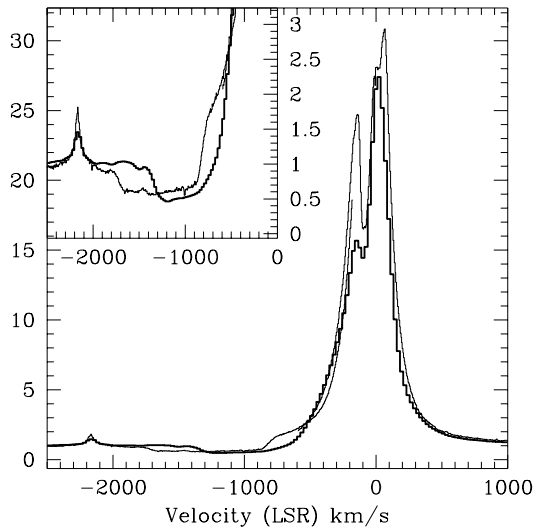
**Figure 1.** The Hα line in January (thick line) and April 1997 (thin line). The insert in the top left-hand corner is a magnification around the P Cyg absorption. The bluest emission peak is the Fe II λ6517 line.



**Figure 2.** The hydrogen recombination lines. For clarity, the Hα and Hβ lines have been multiplied by 30 respectively 4 to enhance the absorption. The vertical lines indicate the central velocities of the Hα emission peaks.

other lines are visible, most notably lines of [O I] and several strong Fe I lines. In some He I lines emission is accompanied by broad absorption. Diffuse interstellar bands (DIBs) are present in absorption. In Figs. 1, 2, 3 and 4, several parts of the spectrum are shown. What catches the eye are the very broad blueshifted absorption components in Hα, Hβ and the He I λ 6678 line. The [O I] lines are markedly narrower than the Fe II lines. We find a Local Standard of Rest (LSR) velocity of $-17 \pm 4$ km s$^{-1}$ from the Fe II and [O I] lines. We take this figure to be indicative of the system's radial velocity.

The emission in Hα is double-peaked and displays broad wings. The broad P Cygni type absorption extends to an unprecedented blueshifted edge velocity of 1800 km s$^{-1}$ with respect to the systemic velocity. The broad absorption in the He I λ6678 line indicates that this high excitation line is also formed in a circumstellar outflow. As there are no bona fide photospheric absorption lines present in the spectrum, it is possible that there is a non-stellar contribution to the optical spectrum. The dearth of photospheric absorption lines extends into the ultraviolet. Based on the many low excitation lines, de Freitas Pacheco et al. (1985) suggested that the UV spectrum is due to a 'cool' wind.

## 3.1 The Balmer lines

Fig. 1 shows an overplot between the January 1997 (thick line) and the April 1997 (thin line) observations. As the free spectral range of the echelle spectrograph was smaller than the total line width of Hα, we show an overplot of the two orders containing the Hα line. Despite problems with the continuum rectification, which was performed independently of the orders covering Hα, the agreement in the overlap region is very good.

The strength of especially the blue emission peak in Hα has appreciably increased in April 1997, as has the strength of the Fe II line at 6517 Å. Perhaps more interesting are the changes in the edge velocities of the Hα absorption component. Whereas in January 1997, the epoch of our spectropolarimetric observations, the maximum absorption blueshift was of order 1500 km s$^{-1}$, reaching in to a minimum velocity of $-600$km s$^{-1}$, this has changed to a velocity range of $-1800$ to $\sim -800$ km s$^{-1}$ in April. The changes are undoubtedly real. Also, since the high resolution April data oversample the spectrum, the edges to the P Cygni absorption are indeed as sharp as they appear to be.

Fig. 2 shows Hα, Hβ and Hγ on the same velocity scales. The higher order Balmer line spectra have been re-binned to pixels of size 0.15 Å to increase the SNR of the spectra. The P Cygni absorption is less deep in Hβ and not necessarily present at all in Hγ. The double emission peaks occur at the same velocities in all three Balmer lines, the velocity difference being 180 km s$^{-1}$ (LSR). This argues against the common hypothesis that the double-peaked appearance of the Balmer line emission betrays formation in a Keplerian circumstellar disk. One would expect that if rotation were the dominant kinematic component in the line-forming region, the velocity difference between the two peaks would increase up the Balmer series as the line forming region is smaller due to the lower line opacity. This is not seen.

In addition, the central reversal in Hα is a little more blueshifted than that in Hβ and Hγ, (respectively –60 km s$^{-1}$ (for Hα) and –30 km s$^{-1}$ with respect to systemic). This is also inconsistent with what would be expected of a purely rotational velocity field. Instead, it is possible that the central reversals are due to self-absorption in a slowly expanding wind.
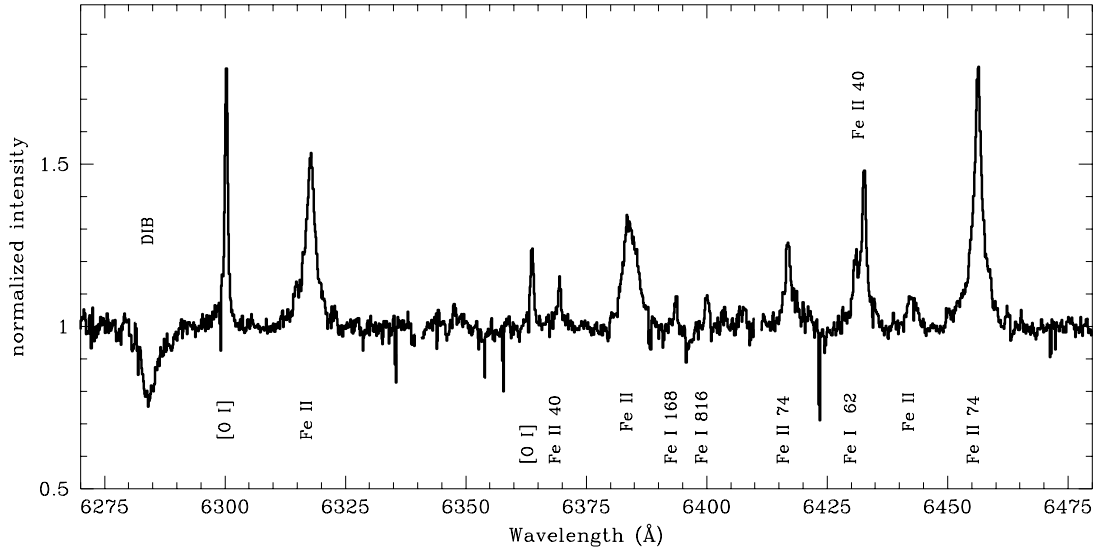
**Figure 4.** A representative part of the April 1997 spectrum, rebinned to 0.15 Å, containing the many different line profiles in the spectrum of HD 87643.
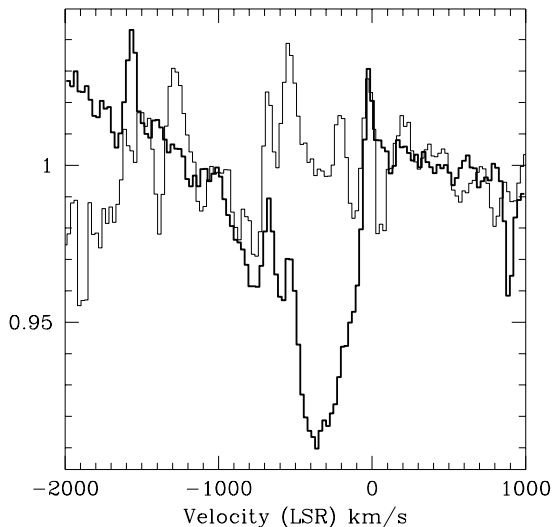


**Figure 3.** As Figure 1, but now for the He I $\lambda$6678 line. The April spectrum has been smoothed to the same resolution as the January spectrum. The different slopes at the blue end of the spectra are the result of the continuum flattening; the line is located in the red emission wing of H$\alpha$. The emission feature at $\sim$ $-1600$ km s$^{-1}$ in the January data is real, as it appears in both the 31 December 1996 and 1 January 1997 spectra, the line could however not be identified.

## 3.2    Other spectral lines

There is a hint of He I $\lambda$5876 absorption in the April echelle spectrum, but the low SNR prevents any further comment. However, the He I $\lambda$6678 line is clearly present in both spectra (Fig. 3). The April spectrum has been box-car smoothed over 15 pixels, and re-binned to pixels of 0.5 Å to enable comparison with the higher SNR spectrum from January. In January, the $\lambda$6678 line showed a faint narrow emission (at $-16$ km s$^{-1}$) accompanied by a broad P Cygni type absorption with a terminal velocity of $\sim$ 1100 km s$^{-1}$. This velocity is somewhat lower than found in the H$\alpha$ line. The changes between January and April are qualitatively like those observed in the H$\alpha$ line; the low velocity absorption has disappeared in the April data, but there are hints that both the emission and a part of the high velocity absorption at about $-900$ km s$^{-1}$ are still present.

To illustrate the different heavy element emission line profiles that are present in the optical spectrum of HD 87643, we show the wavelength range $6275 - 6475$ Å in Fig. 4. Beyond the conspicuous DIB in absorption at 6284 Å, the [O I] doublet at 6300 and 6363 Å, and a host of Fe II lines and some Fe I lines appear. Both [O I] lines peak at $-14$ $\pm$ 5km s$^{-1}$, with a FWHM of 40 km s$^{-1}$, while most Fe II lines have peak velocities between $-14$ and $-22$ km s$^{-1}$, and are much broader, with FWHM of order $100 - 150$ km s$^{-1}$. However these larger FWHM values are under half those of the Balmer lines. Some weak Fe II lines and the Fe I lines have FWHM comparable to the sharp [O I] lines.

Based on the observed line profiles in its spectrum, it would seem that the circumstellar medium of HD 87643 consists of three kinematic components: firstly, a very strong, high velocity wind with outflow velocities in excess of 1000 km s$^{-1}$ that the hydrogen and helium lines sample; secondly, a slower outflow traced by the broad Fe II lines and H I core emission; and lastly, the narrow forbidden lines, narrow Fe I lines and some weaker Fe II lines, constitute a third component that may be due to a much larger low-density nebula around the star.
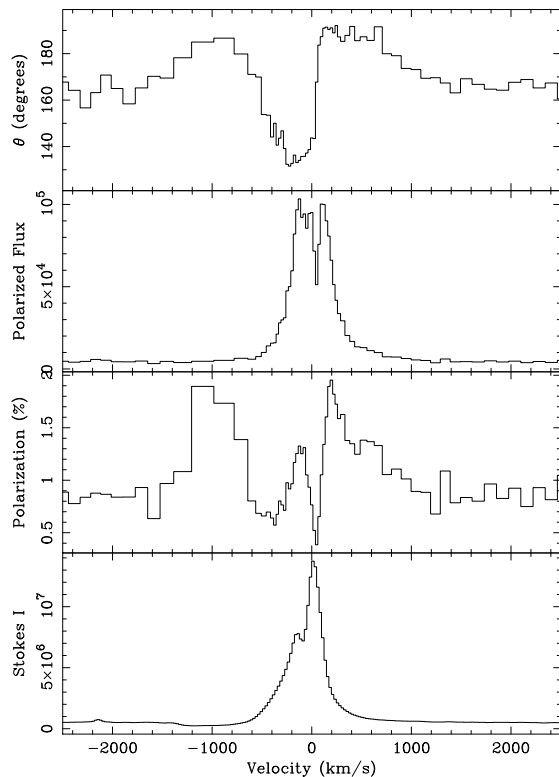
**Figure 5.** The polarization spectrum around Hα. The spectrum has been rebinned such that the individual pixels have 1σ uncertainties in polarization of 0.1% .

# 4   POLARIZATION

Within the error-bars, the polarization characteristics of the 31 December 1996 and 1 January 1997 spectra are equal. The linear polarization spectrum around Hα is shown in Fig. 5. The panels show, from bottom to top, the total intensity spectrum, the polarization percentage, the polarized flux (i.e. intensity times polarization) and the polarization angle.

The observed polarization is enhanced in the P Cygni absorption and along much of the emission profile. In the polarized light spectrum, the enhanced polarization in the absorption component has disappeared. Since polarization changes across Hα are present, one can already conclude two things; firstly, the main mechanism that causes the polarization does not act equally on line and continuum and so must act within the line forming region, ruling out scattering by small dust particles, visible in the near-infrared excess. Secondly, the projection of this region onto the plane of the sky is not circularly symmetric.

Obviously, the observed polarization includes contributions of unknown magnitude from interstellar polarization and, possibly, circumstellar dust. The effects of both on the resulting polarization spectrum are not simple. However, the situation presented in QU space (rather than in the wavelength domain) is easier to grasp since the interstellar polarization component on its own must add the same (Q,U) vector to all points. Circumstellar dust polarization can also

be considered constant over the narrow wavelength range of the spectrum, and so the same consideration applies.

Fig. 6 shows the Hα spectrum in (Q,U) space. For clarity, several cuts along the velocity range (LSR) have been made. The first panel shows the (Q,U) vectors over the velocity range $(-2500$ km s$^{-1}$,2500 km s$^{-1})$ covering the Hα line and part of the continuum. The clustering of points at (1%,–0.5%) represents the continuum points, while the polarization across Hα follows a loop in the (Q,U) plot. The subsequent panels break this loop up into segments.

The presence of the loop allows us to measure the position angle of the scattering material with relative ease in (Q,U) space. As the contribution from circumstellar dust (and interstellar polarization) amounts to a constant offset in the figure, the position angle can be measured from the slope of the loop. The overall angle $\Theta = 0.5 \times \mathrm{atan}(\Delta U/\Delta Q)$ $\sim 20^{\mathrm{o}}$ can be identified with the intrinsic polarization angle of the scattering material.

## 4.1   Interstellar polarization

The main uncertainties in determining the intrinsic polarization of an object are caused by the unknown value of the superimposed interstellar polarization (ISP). An additional problem in our case is the unknown circumstellar dust polarization. In the following we discuss the ways in which it is possible to obtain a value of the ISP.

### 4.1.1   Field stars and polarimetric variability

Assuming that stars in the neighbourhood of the target star are not intrinsically polarized, one can in principle argue that their observed polarization is representative of the ISP suffered by the target. To this end, we have searched the polarization catalogue by Matthewson et al. (1978). Within a radius of 200′ of HD 87643, 59 objects were found. However, their polarization angle and the polarization percentage vary considerably. The average polarization and angle of the total sample is 1.34 ± 0.82% and 119 ± 32$^{\mathrm{o}}$. We selected several subsamples of objects using either $A_V$ or the distance modulus as criteria, but the standard deviations on the means did not improve significantly. Consequently, the field stars are best used as a consistency check rather than as the direct means for determining the ISP. Furthermore, this technique can not provide a correction for the circumstellar dust contribution to the polarization.

The polarimetric variability is an alternative method to separate the intrinsic polarization from the ISP. As the variable polarization is due to the intrinsic polarization, one expects the polarization to move along a straight line in (Q,U) space, thereby defining the intrinsic polarization angle. Broad-band polarimetry is provided by Barbier & Swings (1981), Gnedin et al. (1992) and Yudin & Evans (1998). However, the number and quality of the data-points is not sufficient to improve upon the 20$^{\mathrm{o}}$ found earlier.

### 4.1.2   The 'unpolarized' Hα method

The field-star method and the polarimetric variability serve to illustrate the problems commonly encountered in correcting for the ISP superposed on polarimetric data. Our last
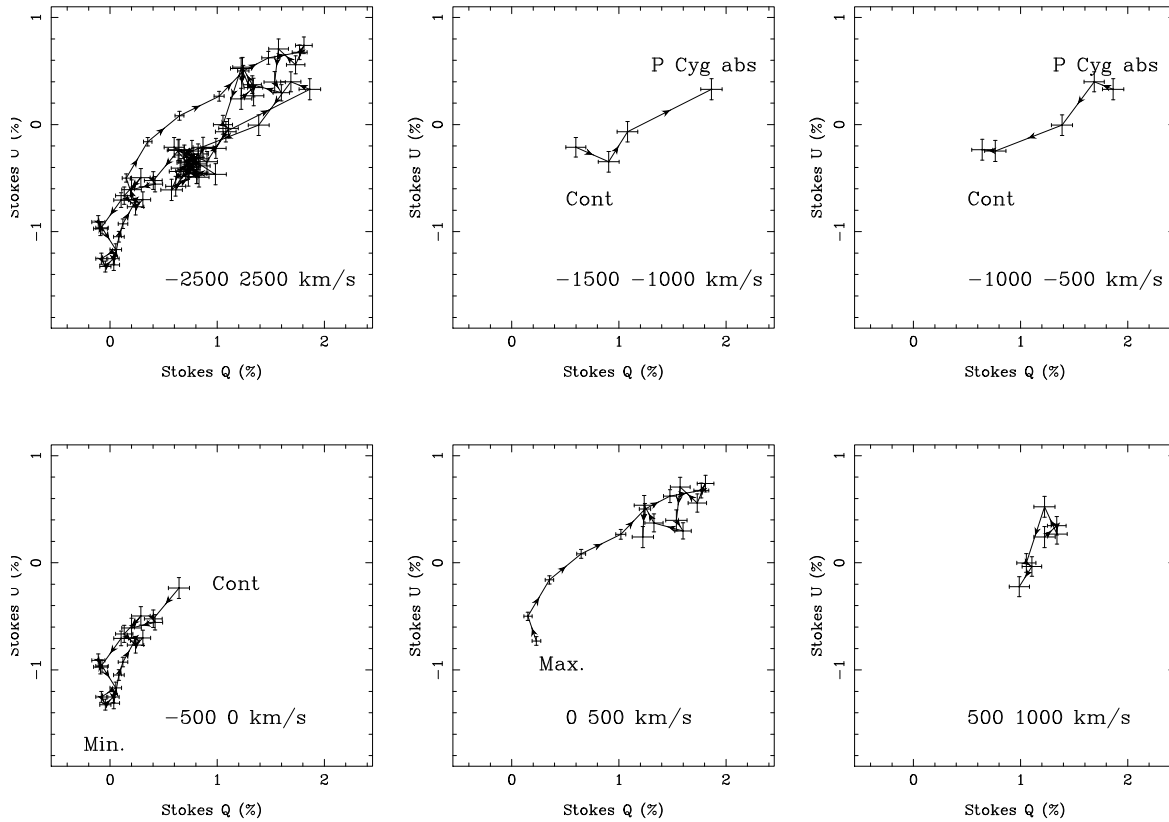
**Figure 6.** The Stokes QU vectors across Hα in HD 87643. The spectra have been rebinned such that the QU vectors have 1σ errors of 0.1%. The panels show different parts of the spectrum as function of velocity (LSR), which are indicated in the bottom of each panel. Particular locations in the spectrum are labeled. The first panel includes data from across the whole line profile and a portion of the continuum. The next two panels show the behaviour across the P Cyg absorption, the polarization changes with a relatively constant Θ of 20° and returns to the continuum polarization as the wavelength increases. Then, with increasing emission, the polarization changes with an opposite sign but at the same angle until the central reversal in the Hα line at –80 km s⁻¹ is reached at (0%,–1.4%). From then (next panel) the angle changes somewhat but the polarization reaches the same values as for the P Cygni absorption at the red emission peak at +20 km s⁻¹, to return to the continuum value as the emission wing reaches the continuum.

resort is to assume that the Hα emission itself, at some wavelength within the profile is intrinsically unpolarized. Since this does not necessarily have to be the case, there is clearly scope for this to be an over-simplification. However, this method also has the advantage that a correction is made at once for both the circumstellar dust contribution and the interstellar component.

Usually, the correction is made by measuring the polarization at the line emission peak. But as can be seen from Fig. 5, the line peak is at a wavelength where the polarization is very sensitive to wavelength, making it difficult to choose a well-constrained ISP correction. Fortunately, we know from the slope in the QU diagram (Fig. 6) that the intrinsic position angle should be close to 20°. We may also assume that the Hα emission is less polarized at the systemic velocity, given the narrow nebular component of emission associated with this object that is signalled by the [O I] lines. We therefore chose to use an iterative procedure to arrive at the most likely value of the ISP. We derived the intrinsic polarization for every point in QU space close to the systemic velocity, assuming that the observed polarization is due to interstellar and circumstellar dust. For all points

close to the local minimum in the emission line, we found resulting intrinsic polarization angles close to 20°. The point at (Q=0%, U = –1.2%) resulted in an intrinsic angle of 24 ± 1°. This point corresponds to an interstellar polarization of 1.2% at an angle of 135°, which is in fair agreement with the field stars (see above). The wavelength is 40 km s⁻¹ (less than one resolution element) blueshifted from the systemic velocity. We will adopt this point as representative of the superposed dust polarization.

The resulting intrinsic polarization spectrum is shown in Figure 7. The polarization runs much more smoothly along the line profile, suggesting that the ISP has much to do with the appearance of the observed spectrum. If the ISP is measured in points close to the chosen QU point, the resulting intrinsic polarization spectrum is almost unchanged. The polarization level across the spectrum changes by less than few tenths of a percent, and the rotation angle in the continuum changes by a few degrees. However, the rotation angle through the Hα line centre changes considerably; the peak angle changes from 150° for (0,–1.2%) to 45° for (0,–1.4%).
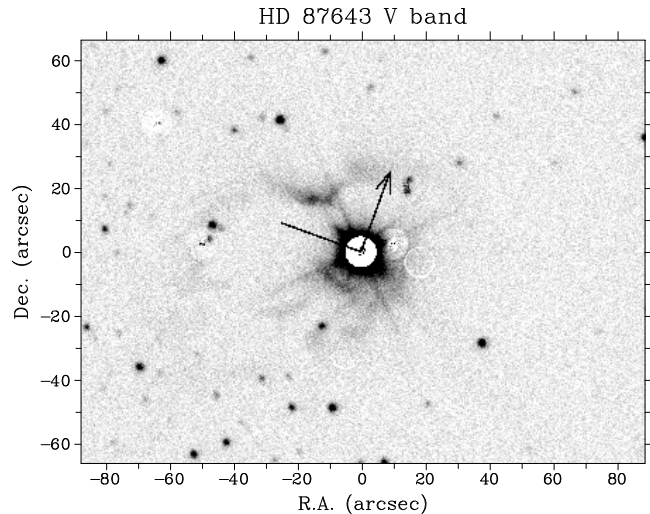
The P Cygni absorption component still exhibits a
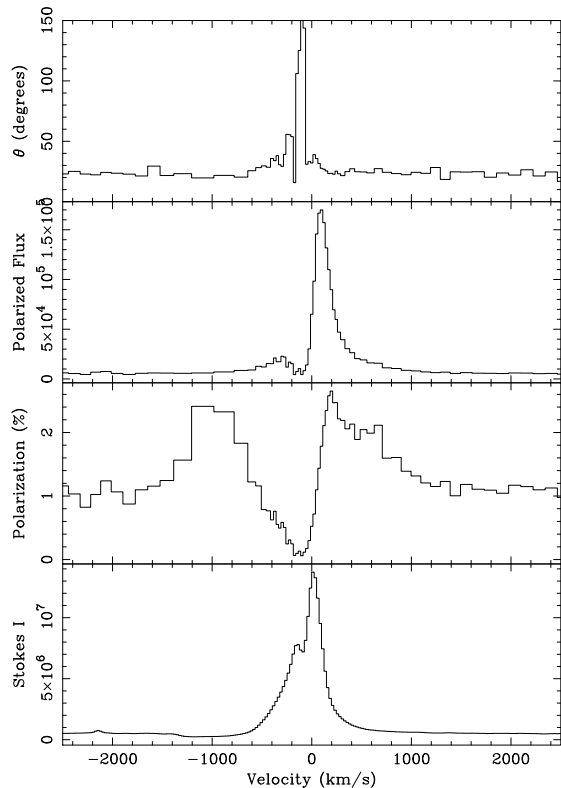
**Figure 7.** The intrinsic polarization spectrum around Hα obtained by correcting the observed spectrum for a combined interstellar and circumstellar polarization vector (Q,U) = (0,–1.2%).



**Figure 8.** The nebula of HD 87643 in the *V* band. North is at the top, while East is to the right. The brightest field stars have been removed, and the central star has been masked to enhance the faint structures. The arrow represents the intrinsic polarization angle of 20°.

higher percentage polarization than the adjacent continuum, although there is no change in polarization angle across this part of the line profile. Despite the problems in obtaining the intrinsic Hα polarization spectrum, it is clear that the line-wings are more polarized than the continuum and that the overall wavelength dependence does not simply mimic the intensity profile.

## 4.2 The geometry of HD 87643 on larger scales

The extended nebulosity of HD 87643, observed in the *V* band is shown in Fig. 8 where the nebula is readily visible. Extended nebular emission was detected in both the *R* and *V* images, and was more intense in the latter. Similar nebular structures around HD 87643 were not detected in the narrow-band Hα and [S II] images. This confirms the reflection status of the material as suggested by Surdej et al. (1981).

The geometry of the nebula is quite complex. Several components of the nebula are visible. There is an extension in the NNE direction, which seems to have a counterpart, albeit much closer to the star, in the SSW direction. This may be evidence for multiple mass outbursts, but deeper images are needed to appreciate such structures around the star. Perpendicular to this NNE-SSW component, is a larger extension which is only present in the WNW direction. The NNE-SSW component seems to be aligned with the position angle of the intrinsic polarization vector, with the western

structure almost perpendicular to it. It may very well be that the circumstellar material around HD 87643 repeats the same geometry on both large scales (the reflection nebula) and small spatial scales (seen in the Hα polarization).

## 5 ON THE NATURE OF AND DISTANCE TO HD 87643

As the distance to HD 87643 and, by implication, the star's evolutionary status, is not yet a settled question, a reassessment of its value is appropriate. We will show below that, based on the magnitude of the interstellar extinction and kinematics, HD 87643 is more likely to be an evolved object than a young star.

### 5.1 Magnitude of interstellar extinction

The extinction to HD 87643 can be determined in several ways:

(i) For a spectral type of B2V, the total *E(B–V)* found by de Freitas Pacheco et al. (1985) is 0.63 mag. This value should not be greatly dependent on the assumed spectral sub-type within the early-B range. However, given the problems that inevitably arise in fitting the spectral energy distributions of significantly reddened stars, this issue may benefit from a fresh examination

(ii) The strength of the Na D absorption components (total EW 0.75 and 0.55 Å for the D2 and D1 lines respectively) would indicate a relatively large interstellar *E(B–V)*. One should however be cautious in interpreting the total EW of Na D absorption. In a recent study of the strength of the Na D1 absorption as a function of reddening by Munari & Zwitter (1997), the EW shows a linear dependence on reddening at small EWs, while the dependence flattens for larger EW,
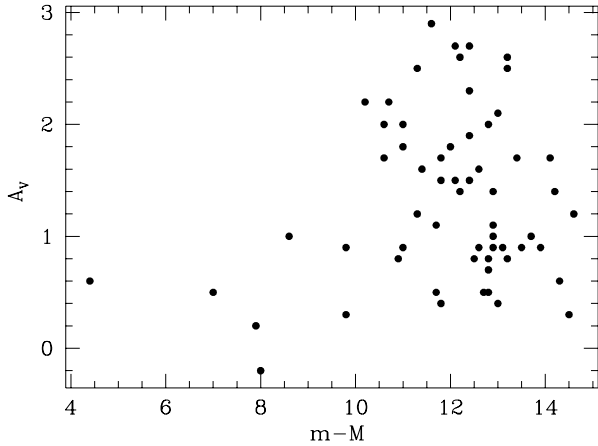
**Figure 9.** $A_V$ as function of distance modulus for all stars in the Matthewson et al. (1978) catalogue of polarized stars within $200'$ from HD 87643.



**Figure 10.** Na D1 & D2 lines in the line of sight towards HD 87643 The systemic velocity of the star is also indicated.

in a sense, this is a simple curve-of-growth effect, where saturated lines need higher column densities than the linear part would imply.

Taking into account the multiple components in the Na D lines we arrive at a low $E(B{-}V)$ of $0.2 \pm 0.15$. The caveat in this approach may be that circumstellar emission components would artificially give the impression of multiple components. However, taking the data as they are, we arrive at a low value for the $E(B{-}V)$.

(iii) The few Diffuse Interstellar Bands (DIBs) that are visible in our spectrum suggest a larger $E(B{-}V)$. The EW of the $\lambda5780$ DIB is 0.3 Å, which corresponds to $E(B{-}V) =$ 0.51, based on the calibration EW-$E(B{-}V)$ provided by Jenniskens & Désert (1994). Other DIBs in the spectrum result in the same values for $E(B{-}V)$: EW($\lambda5795{+}5797$) = 0.18 Å ( $\rightarrow$ $E(B{-}V) = 0.72$) and $\lambda6284$ (combined 6281 and 6284; 1.05 Å $\rightarrow$ $E(B{-}V) = 0.57$) ). Since DIBs are weaker in the spectra of stars of which it is known that much of the line-of-sight extinction originates in their circumstellar shells, it is generally accepted that much of the extinction traced by DIBs is interstellar (see the discussion by Oudmaijer, Busfield & Drew 1997, and references therein). Assuming that this applies to HD 87643 as well, the interstellar extinction towards HD 87643 traced by the DIBs has a value $E(B{-}V)$ $\sim 0.6$, or an $A_V \sim 1.9$, for a ratio of total-to-selective extinction, $R_V$, of 3.1. This agrees well with the total $E(B{-}V)$ as de Freitas Pacheco et al. found based on the reddening of the spectral energy distribution, but does not agree with the lower $E(B{-}V)$ based on the Na D1 line.

From the above, we find that the determination of the interstellar extinction to HD 87643 is ambiguous, the DIBs would imply a $E(B{-}V)$ of order 0.6, while the Na D components may imply a lower $E(B{-}V)$. This may be compared with the interstellar extinction towards nearby stars. The polarization catalogue compiled by Matthewson et al. (1978), discussed earlier, also contains values for the extinction and photometric distances of more than 7500 objects. For the stars within $200'$ from HD 87643, we find from Fig. 9 that $A_V$ of order 1.9 suggests a distance modulus of order $10-14$ ($1-6$ kpc), while for lower values of $A_V$ the distance modulus can be anything between 0 and 15 magnitudes.
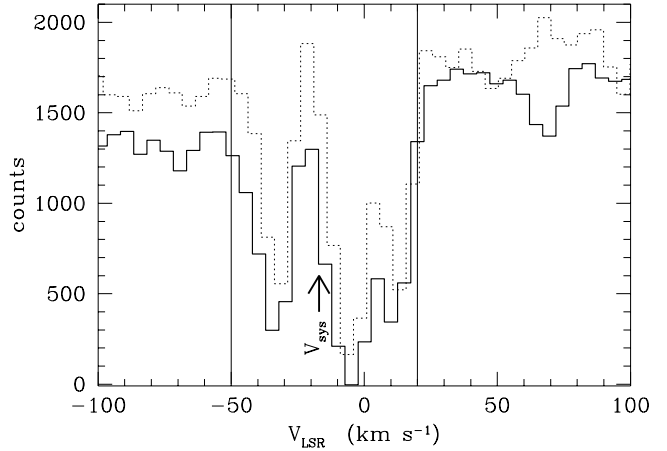
## 5.2 Kinematic information

Let us now consider the location of the object in the Galaxy. The object projects onto the sky close to the tangent edge of the Carina spiral arm in the outer Galaxy. At this particular longitude, the distance to the near side of the Carina arm is estimated to be of order $1.5 - 3$ kpc, while its far side extends to more than 10 kpc from the Sun (Cohen et al. 1985, Grabelsky et al. 1987). The CO and H I maps of Grabelsky et al. (1987) indicate that the intervening local material, the near side and far side of the Carina arm are relatively well separated in velocities. The local material has LSR velocities roughly between –9 to 7 km s$^{-1}$, while the near side of the Carina arm, overtaking the Sun, is moving at more negative velocities (at least to $\approx$ –35 km s$^{-1}$ at the longitude of HD 87643), and the far side, trailing the Sun, is located at more positive velocities (to $\approx$ + 40 km s$^{-1}$).

Assuming that the Na D absorption is interstellar, we can use the kinematics of the Na D absorption components to estimate the location of the star in this sightline. The Na D1 and D2 lines from the echelle spectrum are shown on top of each other in Fig. 10. Three distinct absorption components can be identified at –35 km s$^{-1}$, –9 km s$^{-1}$ and +10 km s$^{-1}$ in the LSR frame. The vertical lines indicate the entire velocity coverage, which ranges from –50 to +20 km s$^{-1}$. The range of velocities spanned by the Na D absorption suggests that HD 87643 lies in the nearer half of the Carina arm.

If the interstellar extinction, $A_V$, is greater than 1, a broadly consistent picture of HD 87643 at a distance of $\gtrsim 2$ kpc emerges. For an average $V$ magnitude of 9, the intrinsic $m_V$ lies in the range –2.9 to –6.9 for a distance range $1 - 6$ kpc. The bolometric correction for an early B-type star is of order –2.5 (Straižys & Kuriliene 1981), so the bolometric magnitude of HD 87643 would range between $\sim$ –5.4 to –9.4 (corresponding to luminosities between 10 000 and 400 000 L$_\odot$ ). The higher luminosities are in the neighbourhood of those of B-type supergiants, but the lower end can be occupied by both main sequence objects and lower luminosity B[e] stars in the Magellanic Clouds (Gummersbach, Zickgraf & Wolf 1995). There is even a slight possibility that HD 87643 is a low mass post-AGB star.

### 5.3 HD 87643 as an evolved B[e] star

The balance of probabilities on the question of the distance to HD 87643 is in favour of its being a (somewhat) evolved luminous object, rather than a very young star (an opinion previously expressed by e.g. McGregor et al. 1988). In this respect this star may prove to be related to the so-called B[e] supergiants in the Magellanic Clouds (see Zickgraf et al. 1985, 1986, 1996 and references therein). It is thus far not very clear whether these objects can be linked to the Luminous Blue Variable phase of evolution, or how they link to any other phase (e.g. Schulte-Ladbeck 1998; Zickgraf 1998).

The B[e] stars exhibit hybrid spectra, with mostly very broad wind absorption in the UV resonance lines, no photospheric absorption lines, very broad hydrogen recombination emission lines, with absorption components at small velocities, and a host of narrow permitted and forbidden lines of singly ionized iron. HD 87643 fits in with this description. The generally accepted model for these B[e] objects was devised in 1985 by Zickgraf et al. (see also Zickgraf et al. 1986). It describes these objects as having a two-component wind. Fast outflows are thought to originate in a line-driven polar wind, while the narrower lines are formed in a relatively slowly rotating, slowly expanding circumstellar disk. The presence of disk-like structures around these objects was strengthened with the polarimetric observations of Magalhaes (1992) which showed that the B[e] supergiants have strong intrinsic polarizations.

HD 87643 stands apart from the Magellanic Cloud B[e] supergiants in a number of respects. Usually, fast wind component speeds up to $\sim 1000$ km s$^{-1}$ are only visible in UV resonance lines, while the slow wind component is thought to be traced by the optical emission lines. For example, the H$\alpha$ line profiles of the B[e] supergiants do not typically show P Cygni absorption at velocities larger than $\sim 100$ km s$^{-1}$ – hence the absorption is attributed to disk expansion alone. The presence of both a broad blueshifted and a narrow, nearly central absorption component in H$\alpha$ and H$\beta$ in HD 87643's spectrum is thus abnormal. Somehow, in HD 87643 the fast-wind H I column density is greatly in excess of typical values.

A further point of interest is that the forbidden lines are narrower (FWHM of order 40 km s$^{-1}$) than the velocity typically inferred for the 'slow' winds (FWHM of 100 – 150 km s$^{-1}$ for the FeII lines). The data of Zickgraf et al. (1986) for the LMC stars hint at different outflow velocities as well, but not as clearly as for HD 87643. This indicates that low-density nebular emission constitutes a third component which may, perhaps, trace the expanded remnant of a previous mass loss phase of the star. This third physical component might also give rise to the far-infrared excess.

### 5.4 Significance of the H$\alpha$ polarization

The complex behaviour of the linear polarization across the H$\alpha$ line contains information, over and above that available from direct spectroscopy, on the kinematics of the immediate circumstellar medium of HD 87643.

Probably because of the limited use of high resolution spectropolarimetry, only few instances have been reported in the literature concerning enhanced H$\alpha$ polarization, or changes along the H$\alpha$ line profile itself: the symbiotic system BI Cru has an enhanced H$\alpha$ line polarization (Harries, 1996), Harries & Howarth (1996) found enhanced polarization in the H$\alpha$ line centre of the O supergiant $\zeta$ Puppis, while Schulte-Ladbeck et al. (1994) showed that the line wings in the H$\alpha$ line of the Luminous Blue Variable AG Car have a different polarization signature than either the line centre or the continuum.

A clue to the origin of the observed polarization characteristics of HD 87643 may be provided by model predictions of electron-scattering geometries. A start in developing such models has been made by Wood, Brown & Fox (1993), who calculated the polarization characteristics of rotating and expanding disks around stars. Although their schematic model does not include radiation from the circumstellar material itself, their results provide insight into the polarization expected from such disks.

Wood et al. (1993) present the expected polarization due to a scattering rotating disk - viewed at various inclination angles - and find that this results in equally polarized blue and red emission, and, because of the left-right anti-symmetry of the velocity field from the observer's (and scatterer's) point of view, a flip in rotation angle from one peak to the other. In contrast to this, a purely expanding disk results in enhanced polarization in the red emission peak – a response to the monotonic expansion of the atmosphere – and a net decrease in the blue wing. There is no angle rotation in this case as the velocity field seen by the observer is instead left-right symmetric. Neither of these cases describes, even qualitatively, the polarization of H$\alpha$ in HD 87643. However, in the case of a hybrid velocity field in which rotation and expansion are both present, Wood et al.'s model results do come close to our observations. The model shows enhanced polarization on both sides of the line profile, with the red peak slightly more polarized than the blue peak, while the angle rotation only takes place near line center. The only respect in which this pattern differs from that in HD 87643 is that the blue and red peaks in the polarization percentage are almost matched.

Encouraged by Wood et al's models, one may deduce, qualitatively from the polarized flux spectrum (Fig. 7, in which the blueshifted peak is much weaker than the redshifted) that the scatterers 'see' mainly expansion with only a modest component of rotational motion mixed in. For the timebeing this result on H$\alpha$ points the way toward the correct dynamical model for B[e] stars. Eventually it will afford an important quantitative test.

## 6 A RADIATION-DRIVEN DISK WIND MODEL FOR HD 87643 AND OTHER B[E] STARS

The two-component wind model of Zickgraf et al. (1985) explains the observed characteristics of B[e] stars very well in a qualitative way, without specifying the underlying dynamics. The fast polar flow is easily understood as a normal line-driven wind. The difficult issue that has stood in the way of a complete dynamical description is the cause of the slow equatorial flow. In recent years models have been proposed in an attempt to deal with this, the focus being upon the production of a slow wind direct from the surface of a rapidly rotating star. Here we set aside the basic difficulty of
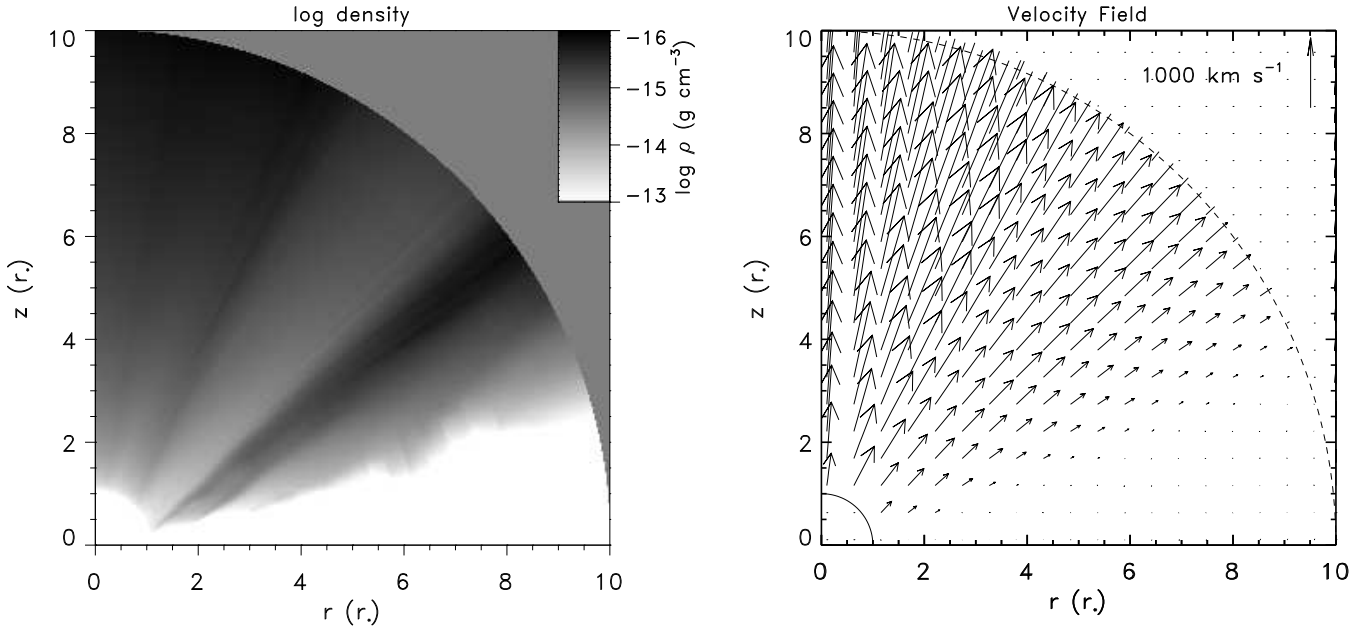
**Figure 11.** The grey-scale density map and velocity field for a model of a B[e] supergiant with an accretion disk, described in the text (left and right hand side panels). To make the density changes in the map more visible, we set the disk density to be not higher than $10^{-13}$ g cm$^{-3}$. The rotational axis of the disk is along the left hand side vertical frame, while the disk midplane is along the bottom horizontal frame. Note that the right hand side panel does not show the rotational component of the velocity.

producing the slow equatorial flow from the star along side the fast polar wind. Instead we investigate the consequences of *assuming* there is a Keplerian circumstellar disc that may also be a source of mass loss. We then show that the model's properties offer considerable promise of explaining what is observed in B[e] stars such as HD 87643.

Whatever the dynamical origin of a disk structure in B[e] stars and similar objects, it is interesting to determine the system properties when the presence of a disk is assumed a priori. Proga, Stone & Drew (1998) have begun such a study. Originally aimed at explaining the properties of mass loss from cataclysmic variables, their hydrodynamic model of radiation driven winds from accretion disks has much wider application. For example, Drew, Proga & Stone (1998) have adapted and extended the model to describe massive young stellar objects (YSOs).

Here, we assume that an optically-thick disk exists around a B star for reasons unknown, and that it shines by virtue of reprocessing the stellar radiation falling upon it. The star itself is non-rotating, a convenient assumption rather than one that defines the model (see later). The disk is geometrically thin in the sense that the reprocessed stellar radiation is emitted from the disk mid-plane. Each point on the disk is assumed to emit isotropically. The main input parameters for the 2.5-dimensional line-driven wind model are the stellar parameters: mass 25 M$_\odot$, radius 25 R$_\odot$, and luminosity $10^5$ L$_\odot$ (a luminosity in the middle of the range discussed by Gummersbach et al. 1995). Unless specifically mentioned, the model parameters are as in Table 1 of Drew et al. (1998).

To calculate the structure of a wind from the star and the disk, we take into account stellar gravity, gas pressure

effects, rotational and radiation forces. We hold the fluid temperature constant at 15000 K in our isothermal equation of state. We use the CAK force multiplier (Castor, Abbott & Klein 1975) to calculate the line-driving force. In this approximation, a general form for this force is:

$$F^{rad,l} = \iint_\Sigma \left( \frac{\sigma_e d\mathcal{F}}{c} \right) M(t). \tag{1}$$

The term in brackets is the electron scattering radiation force and $M$, the force multiplier, is the increase in opacity due to spectral lines. The integration is over all visible radiating surfaces ($\Sigma$). Our formalism allows the radiation from the central accreting star to be included both as a direct contributor to the radiation force and as an indirect component via disk irradiation and re-emission. Note that $d\mathcal{F}$ contains the total frequency-integrated intensity emitted at any given location. We adopt the simple form for $M$ which still underpins much modelling of OB star winds, i.e. $M = kt^{-\alpha}$, where $t$ is proportional to the local density divided by the local velocity gradient, and $k$ and $\alpha$ are constants (taken to be 0.3 and 0.5 respectively). These calculations have been performed as described for massive YSO's in Drew et al. (1998). Some modifications are needed to accommodate a lower gravity, higher luminosity B[e] star, these are outlined below,

The boundary conditions are the same as in Drew et al. (1998; see also Proga et al. 1998), except for the boundary density along the disk mid-plane and stellar surface. By holding the temperature of the gas constant, the pressure scale height particularly in the outer parts of the disk is artificially high. In previous models the density, $\rho$, along the disk mid-plane was independent of radius, $r$. Here, the combination of constant gas temperature with a markedly lower

stellar gravity gives rise to an over-thick disk atmosphere. To be consistent with the assumption of a geometrically thin disk in this circumstance, it is necessary to modify the density in the disk mid-plane such that it declines with increasing disk radius. We choose $\rho \propto r^{-\frac{21}{8}}$. Such a scaling of the boundary density with radius mimics the radial gas pressure gradient appropriate to a steady-state disk (e.g. Carr 1989). For the disk boundary density at one stellar radius, we adopt $10^{-9}$ g cm$^{-3}$, which is also the density assumed along the stellar surface.

Because the stellar luminosity in our model is about 10% of the Eddington luminosity, we have to take steps to ensure that the radiation pressure due to electron scattering does not, unphysically, take effect inside the dense disk where in reality it should be negligible in the presence of a nearly isotropic radiation field. It is not negligible only because of our simplification that the radiation field streams freely from the disk and stellar boundaries. We have found that this is most problematic in the inner disk where the radial force term due to the stellar flux can be large if it is not corrected for radiation transfer effects. The device used to remove this difficulty is to attenuate the stellar flux in the radial electron-scattering radiation force integral by multiplying it by $e^{-\tau_{es}^r}$, where $\tau_{es}^r$ is the optical depth in the radial direction. We approximate the optical depth by

$$\tau_{es}^r = \sigma_e \, \rho_{Disk} \, \delta r_{Disk} \qquad (2)$$

where $\sigma_e$ is the mass scattering coefficient of free electrons, $\rho_{Disk}$ is the density of the disk in hydrostatic equilibrium, and $\delta r_{Disk}$ is the pressure scale length of the hydrostatic disk. We calculate $\delta r_{Disk}$ using Proga et al.'s equation (11) defining it to be the density $e$-folding length at fixed polar angle, $\theta$.

Finally, it should be emphasised that the disk in our model is best thought of as simply a reservoir of material in Keplerian orbits that is also optically-thick and therefore capable of intercepting and re-radiating the stellar light falling on it. In principle, the radial density gradient across the disk surface can be chosen at will if all orbits within the disk are viewed as non-interacting. We have chosen instead, partly for pragmatic reasons, to adopt a steady-state configuration that would be appropriate to either accretion or excretion.

## 6.1 Results of the model

Figure 11 shows the grey-scale density map and velocity field of our model. Our hydrodynamic calculations show that the radiation pressure due to lines produces a fast stellar wind in the polar region and a slow wind near the equator. Thus, this wind model very much resembles the two-component wind model proposed by Zickgraf et al. 1985 (see also Zickgraf et al. 1989). The main difference between Zickgraf's conceptual model and our quantitative dynamical calculation is that the latter incorporates a zone at intermediate latitudes wherein the stellar outflow is compressed both because of the volume taken up by the disk wind component, and because of the additional component of vertically-directed line radiation pressure contributed by the disk. In this region the wind is slower and denser than at the pole (see below).

Figure 12 presents the run of the density, radial velocity, mass flux density, and accumulated mass loss rate as a
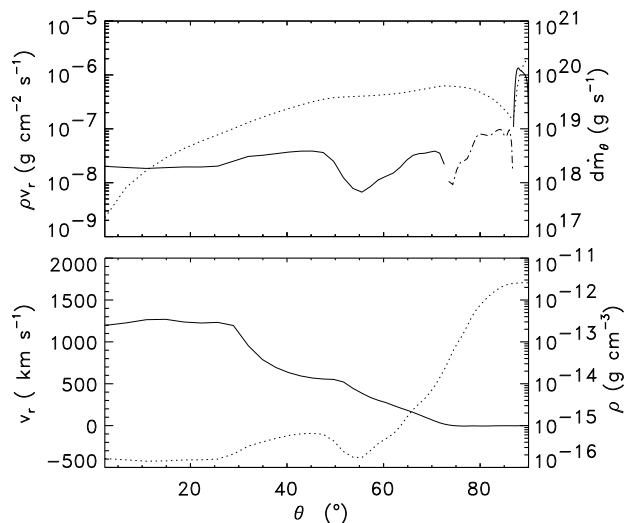


**Figure 12.** Quantities at the outer boundary in the model from Figure 11. The ordinate on the left handside of each panels is marked by the solid line, while the oridinate on the right hand side is marked by the dotted line. The three components of the ouflow are easily distinguished on this figure:1) the 'normal' stellar wind is for $0^o \lesssim \theta \lesssim 20^o$, 2) the disk compressed wind is for $30^o \lesssim \theta \lesssim 50^o$, 3) the slow disk wind is $50^o \lesssim \theta \lesssim 70^o$. The zone for $\theta \gtrsim 70^o$ is where the density profile only slightly deviates from the hydrostatic profile and the matter is a subject of slow velocity oscillations. The gap in the mass flux density is caused by a negative value of $v_r$ for $73^o \lesssim \theta \lesssim 87^o$. We filled the gap by plotting $-\rho v_r$ with a dot-dashed line.

function of the polar angle at the outer boundary, $r_0$, of our model (a distance of 10 stellar radii from the star center). The accumulated mass loss rate is formally:

$$d\dot{m}(\theta) = 4\pi r_0^2 \int_0^\theta \rho v_r \sin\theta \mathrm{d}\theta \qquad (3)$$

The density contrast between the polar regions and $\theta \sim 70^o$, where the radial expansion velocity is $\approx 100$ km s$^{-1}$, is about 2 orders of magnitude. The equatorial wind, originating from the disk, is clearly very much denser and more slowly expanding than the polar flow originating from the star. The mass-loss rates in the two flow components are comparable (see Fig. 12). On the other hand, the stellar wind compressed region at $\theta \sim 45^o$, is denser by a factor of $\sim 5$ and slower by a factor of $\lesssim 2$ than in the polar regions.

## 6.2 Implications of the model

The model calculations yield some interesting results which may begin to explain some of the puzzles in the spectra of HD 87643 and B[e] stars in general.

In the hydrodynamic model described above, irradiation of the optically-thick disk by the star is dynamically important. Without re-processing starlight, the disk on its own could not have promoted outflow from its surface. An effect of irradiation we have not had to treat explitly in the hydrodynamics is the modification of the emergent spectral energy distribution (SED). Let us now anticipate what this might be. Illustrative calculations by Kenyon & Hartmann (1987) showed that the main change due to irradiation on the overall SED is extra emission longward of the stellar

Planck maximum. The excess fluxes at the *J* band found by Zickgraf et al. (1985) may be evidence of this. For B[e] stars, the disk's contribution to the observed continuum can be significant also at optical wavelengths. For example, when a completely flat circumstellar disk around an early B star is viewed close to face on, it may contribute up to half of the *B* band light (see Figure 1 in Drew et al. 1998). A disk of finite opening angle would contribute more. This veiling can go some of the way to explain the observed lack of photospheric absorption lines in HD 87643 and other B[e] stars. In addition, the externally heated disk atmosphere is likely to be a source of heavy element line emission (rather than line absorption) that could serve to cancel out much of the stellar photospheric absorption. For example, Hubeny (1990) shows how strongly irradiated disk atmospheres are characterised by inverted temperature profiles that predispose to net spectral line emission.

A further consequence of the irradiated disk scenario is that the disk can provide a much larger source of background continuum emission which the wind has to shadow to produce net blueshifted absorption in a line such as H$\alpha$. This fact may explain why, in H$\alpha$, the high-velocity absorption is almost flat-bottomed, steep-sided and yet far from black. To grasp this, recall an old result in stellar atmosphere theory that the absorption in an optically-thick purely resonantly scattering transition achieves a maximum depth of half the continuum level (see also Drew 1985). This situation can develop because the line source function is then $WI_c$, where $I_c$ is the background continuum intensity, $W$ is the dilution factor and of course $W \geq 1/2$ within the atmosphere. The same general idea may have some relevance to H$\alpha$ in HD 87643 in that the $n = 2$ level of neutral hydrogen may be well enough populated that resonant scattering is significant, and that the line is forming against a larger than stellar continuum source – with the consequence that the typical dilution factor in the line-forming region is not much below $1/2$.

The new model provides an improved overview as to what may be going on in the line spectrum as a whole. The strong spectropolarimetric signature demands that our viewing angle must be reasonably high. The slowly expanding disk wind component would need to be the origin of the central part of the H$\alpha$ line profile, i.e. the double-peaked emission and the asymmetric dip in between. The somewhat broadened Fe II lines (e.g. in Figure 4) will come from near the base of the disk wind (in keeping with Zickgraf's original concept). The absence of a strong rotational signature in any of the observed line profiles can be accounted for by two cooperating factors – optical depth effects and angular momentum conservation. The majority of lines may be optically-thick, implying that the observed emission samples the outflow (where there is little residual rotation) well away from the star and the disk mid-plane. However, we do know from the H$\alpha$ spectropolarimetry that some rotational motion is detectable. This is very important and very encouraging.

The high velocity blueshifted H$\alpha$ absorption would most likely arise from the compressed stellar wind component. An interesting point about this feature, particularly apparent in the later April observation (Fig. 1), is that it cuts on rather sharply at around $-800$ km s$^{-1}$. This suggests that the density of the absorbing gas is not a monotonic function of the

flow velocity. Our hydrodynamic model shows that such irregularities of the density and velocity are present. As mentioned above, the compressed stellar wind component has densities $\sim 5$ times higher and expansion velocities about half those characterising the radial wind over the pole. At the interface between the compressed stellar wind and the slow disk wind, there is at first a decrease (at fixed radius) in density with increasing polar angle, and then there is a sharp rise again as the disk atmosphere is approached (Fig. 12).

Over this same angular range, the expansion velocity at fixed radius steadily increases. There is thus an absorbing column of higher density. higher velocity material at $\theta \sim 45^o$ along side a column of lower density, lower velocity gas at $\theta \sim 55^o$. Spectral line synthesis is required to investigate whether such a configuration can match the observed H$\alpha$ profiles in HD 87643.

## 6.3    Relation to previous models

The fact of the strong contrast between the polar and equatorial flows implied by observations of B[e] stars obviously demands an underlying geometry that is axial rather than spherical. The introduction of rapid rotation of the star is one way of achieving this. For example, Ignace, Cassinelli & Bjorkman (1996) showed that the 'wind-compressed disk' model (Bjorkman & Cassinelli, 1993) produced for classical Be stars that are known to be rapid rotators, could also apply to B supergiants in the event that they too undergo significant rotation. In this framework, the disk in Zickgraf's concept is seen as a wind compressed zone. Another mechanism that may enable a rapidly rotating star to produce a dense equatorial flow alongside a fast polar wind is the 'bistability' of radiation-driven winds discussed by Lamers & Pauldrach (1991). In this case, the pole/equator contrast arises from latitudinal differences in wind ionization and optical depth. Owocki, Gayley & Cranmer (1998) have reviewed the impact on both models of gravity darkening and non-radial line forces. They conclude that non-radial line forces may prevent the formation of the wind-compressed disk in rapidly rotating hot-star winds. They also provide an expression for the equator/pole density contrast due to bistability operating in the presence of gravity darkening. Using Owocki et al.'s (1998) numbers with $\theta > 70^o$ and a stellar rotation 80% of critical in this expression, we obtain a density contrast of around an order of magnitude at best.

Whilst it is clear that there is more work to be done to confirm the outcome of Owocki et al.'s (1998) analysis, it is certain that stellar rotation on its own cannot *easily* account for the high equator/pole density contrast thought to characterize B[e] stars. However, because our model assumes a significant Keplerian circumstellar disk is already in place, a density contrast of 2 magnitudes or more naturally follows. If the star in our model were a rapid rotator, the important change with respect to the present non-rotating case would be weaker irradiation of the optically-thick disk. In turn this would imply a reduction in the mass loss rate, together with a lower opening angle for the disk wind. Combined, these effects should result in only a small change to the equator/pole density contrast. It is in this sense that stellar rotation is a second-order effect in our calculations.

However, it is a distinct possibility that an optically-thick circumstellar disk only arises where the star is a rapid

rotator – the situation envisaged by the wind-compressed disk and bistability models. If these models do not survive continuing scrutiny, it may prove to be the case that another dynamical process enables B[e] stars to generate optically-thick Keplerian disks around themselves. Given the uncertainty over the evolutionary status of B[e] stars, and the evidence that some may be quite low luminosity objects (Gummersbach et al 1995, see also Drew et al. 1997 on MWC 297), it is also a possibility that some B[e] stars are still in possession of disks created in an earlier evolutionary phase. For example, some may be extreme post-AGB stars that in time will produce bipolar nebulae. Some may be B stars that have not yet dissipated the accretion disks from which they formed. Indeed this could be a solution to the longstanding puzzle, discussed by Herbig (1994), of the phenomenological similarity between B[e] stars and young BN-type objects – perhaps they look the same because they are the same, and disk dissipation timescales are long enough to allow this. The main point of our disk-wind model is that it explores the consequences of an optically-thick circumstellar disk around a B star without first solving the harder problem of its origin.

## 7   CONCLUDING REMARKS

In this paper we have presented an observational study of the B[e] star HD 87643. The observations include high dispersion spectroscopy, medium dispersion spectropolarimetry around $H\alpha$ and imaging. The main conclusions drawn from them are as follows:

(i) From the spectroscopic observations we have found that at least three different line forming regions contribute to the spectrum; a fast outflow giving rise to extremely high velocity components up to 1800 km s$^{-1}$ in $H\alpha$ and neutral helium, a slower outflow visible in the relatively low velocity central reversal absorption in the hydrogen lines and in broad (FWHM $\sim 100-150$ km s$^{-1}$) Fe II lines, while a third, narrow, component (FWHM $\sim 40$ km s$^{-1}$) is revealed by narrow forbidden lines, neutral Fe I lines and some weaker Fe II lines.

(ii) A disk-like structure surrounding the star is revealed by the medium resolution spectropolarimetry. The startling linear polarization changes across the $H\alpha$ emission line immediately imply that there is scattering within the ionized line-forming region and that this volume is certainly not spherical. A comparison with published model calculations shows that a rotating, expanding disk qualitatively reproduces the observed polarization, and illustrates the need for more realistic model calculations.

(iii) Broad-band imaging of the large reflection nebula around HD 87643, suggests that the geometry of the circumstellar material at large scales are comparable to those on the small scales traced in the polarimetry; the intrinsic polarization angle aligns well with the two most conspicuous nebular components.

(iv) Interstellar extinction and kinematic evidence favours a distance to the object of order of several kiloparsecs. This implies that it is unlikely that HD 87643 is a young main sequence object. Nevertheless, these data are not conclusive in deciding whether HD 87643 is a luminous B-type supergiant or a lower luminosity type B[e] star such as those discussed by Gummersbach et al. (1995). Indeed a

feature peculiar to HD 87643 is that the maximum outflow velocities seen in absorption in the $H\alpha$ line ($\sim 1800$ km s$^{-1}$) are significantly higher than those seen in other B[e] stars luminous enough to be classified as supergiants. Since this absorption can only arise in the stellar wind and so may be sensitive to the stellar photospheric escape velocity, a more compact star with a luminosity significantly below that of a supergiant is a possibility.

These results on HD 87643 fit into the general conceptual framework due to Zickgraf et al. (1985,1986) in which B[e] stars are described as the source of two winds – a fast wind in the polar direction and a slower equatorial disk-like wind. Here we have proposed a model that provides a possible physical basis for Zickgraf et al.'s two-wind concept. Our model consists of a star encircled by an *optically-thick* disk wherein radiation pressure is sufficient to power mass loss from both the star and disk. Hydrodynamical calculations yield a fast wind emerging from the star's polar regions and a much slower wind flowing away from the disk. A feature of the calculations not anticipated in earlier qualitative B[e] star models is that the combination of the irradiated disk and its outflow modify the stellar wind at intermediate latitudes, rendering it denser and slower than over the stellar pole. The new picture these calculations present offers considerable promise of explaining our observations of HD 87643. An important next step will be to synthesise spectral line profiles from the model in order to make a direct quantitative comparison with observations.

## REFERENCES

Barbier R., Swings J.P. 1981, IAU Symp. 98 "Be stars", eds. M. Jaschek and H.-G. Groth, p. 103

Bjorkman J.E., Cassinelli J.P. 1993, ApJ 409, 429

Carlson E.D., Henize K.G. 1979, *Vistas in Astronomy* 23, 213

Carr J.S. 1989, ApJ 345, 522

Castor J.I., Abbott D.C., Klein R.I. 1975, ApJ 195, 157

Cohen R.S., Grabelsky D.A., May J., Bronfman L., Alvarez H., Thaddeus P. 1985, ApJ 290, L15

de Freitas Pacheco J.A., Gilra D.P., Pottasch S.R. 1982, A&A 108, 111

de Freitas Pacheco J.A., Faria Lopes D., Landaberry S.C., Selvelli P.L. 1985, A&A 152, 101

Drew J.E. 1985, MNRAS 218, 41P

Drew J.E., Busfield G., Hoare M.G., Murdoch K.A., Nixon C.A., Oudmaijer R.D. 1997, MNRAS 286, 538

Drew J.E., Proga D., Stone J.M. 1998, MNRAS 296, L6

Gnedin IU. N., Kiselev N.N., Pogodin M.A., Rozenbush A.E., Rozenbush V.K. 1992, AZhL 18, 454

Grabelsky D.A., Cohen R.S., Bronfman L., Thaddeus P. 1987, ApJ 315, 122

Gummersbach C.A., Zickgraf F.-J., Wolf B. 1995, A&A 302, 409

Harries T.J. 1996, A&A 315, 499

Harries T.J., Howarth I.D. 1996, A&A 310, 553

Herbig G.H., 1994, in *The Nature and evolutionary status of Herbig Ae/Be stars*, eds. P.S. Theé , M.R. Pérez, E.P.J. van den Heuvel, ASP Conf.Sers. No. 62, p. 3

Hiltner W.A., Stephenson C.B., Sanduleak N. 1968, Astrop. Letters 2, 153

Hubeny I. 1990, ApJ 351, 632

Ignace R., Cassinelli J.P., Bjorkman J.E. 1996, ApJ 459, 671

Jenniskens P., Désert, F.-X. 1994, A&AS 106, 39

Kenyon S.J., Hartmann L. 1987, ApJ 323, 714

Lamers H.J.G.L.M., Pauldrach A.W.A. 1991, A&A 244, L5

Lopes D.F., Daminelli Neto A., de Freitas Pacheco J.A. 1992, A&A 261, 482

Magalhaes A.M. 1992, ApJ 398, 286

Matthewson D.S., Ford V.I., Klare G., Neckel T., Krautter J. 1978, *Bull. Inf. CDS*, 14, 115

McGregor P.J., Hyland A.R., Hillier D.J. 1988, ApJ 324, 1071

Miroshnichenko A.S. 1998, in "Workshop on B[e] stars", eds. A.M. Hubert, C. Jaschek, in press

Munari U., Zwitter T. 1997, A&A 318, 269

Oudmaijer R.D., Busfield G., Drew J.E. 1997, MNRAS 291, 797

Owocki S.P., Gayley K.G., Cranmer S. R. 1998, in *Properties of Hot Luminous Stars*, ed. I. D. Howarth, ASP Conf.Ser. No. 131, p. 237

Proga D., Stone J.M., Drew J.E. 1998, MNRAS 295, 595

Schulte-Ladbeck R.E. 1998, in "Workshop on B[e] stars", eds. A.M. Hubert, C. Jaschek, in press

Schulte-Ladbeck R.E., Clayton G.C., Hillier D.J., Harries T.J., Howarth I.A. 1994, ApJ 429, 846

Stephenson C.B. 1974, ApJ 191, 685

Straižys V., Kuriliene G. 1981, Ap&SS 80, 353

Surdej J., Swings J.P. 1983, A&A 117, 359

Surdej A., Surdej J., Swings J.P., Wamsteker W. 1981, A&A 93, 285

Swings J.P. 1974, A&A 34, L33

Tody, D. 1993, in Astronomical Data Analysis Software and Systems II, A.S.P. Conference Ser., Vol 52, eds. R.J. Hanisch, R.J.V. Brissenden, J. Barnes, p. 173

Torres C.A.O., Quast G., de la Reza R., Gregorio-Hetem J., Lepine J.R.D. 1995, AJ 109, 2146

Wood K., Brown J.C., Fox G.K. 1993, A&A 271, 492

Yudin R.V., Evans A. 1998, A&AS in the press

Zickgraf F.-J. 1998, in "Workshop on B[e] stars", eds. A.M. Hubert, C. Jaschek, in press

Zickgraf F.-J., Wolf B., Stahl O., Leitherer C., Klare G. 1985, A&A 143, 421

Zickgraf F.-J., Wolf B., Stahl O., Leitherer C., Appenzeller I. 1986, A&A 163, 119

Zickgraf F.-J., Wolf B., Stahl O., Humphreys R.M. 1989, A&A 220, 206

Zickgraf F.-J., Humphreys R.M., Lamers H.J.G.L.M., Smolinski J., Wolf B., Stahl O. 1996, A&A 315, 510